Unveiling complex magnetic structures of the 4*f*-4*d* exchange coupled antiferromagnets $Ba_3RRu_2O_9$ (R = Tb, Er)

Deepak Garg [1,*] C. Ritter [2] M. Skoulatos [3] S. Nandi [4,5] and Yixi Su [1]

[1] *Jülich Centre for Neutron Science (JCNS) at Heinz Maier-Leibnitz Zentrum (MLZ), Forschungszentrum Jülich GmbH, Lichtenbergstrasse 1, D-85748, Garching, Germany*

[2] *Institut Laue-Langevin, Boite Postale 156, 38042 Grenoble Cedex, France*

[3] *Heinz Maier-Leibnitz Zentrum (MLZ), Technische Universität München, Lichtenbergstrasse 1, D-85748 Garching, Germany*

[4] *Forschungszentrum Jülich GmbH, Jülich Centre for Neutron Science (JCNS-2), 52425 Jülich, Germany*

[5] *RWTH Aachen, Lehrstuhl für Experimentalphysik IVc, Jülich-Aachen Research Alliance (JARA-FIT), 52074 Aachen, Germany*

(Received 8 December 2025; revised 19 February 2026; accepted 31 March 2026; published 28 April 2026)

The magnetic structures of $Ba_3RRu_2O_9$ (R = Tb, Er) have been investigated using high-intensity neutron powder diffraction (NPD) supported by dc and ac susceptibility studies. The NPD data reveal antiferromagnetic (AFM) ground states below $T_N \sim 9.8$ and 6 K in $Ba_3TbRu_2O_9$ and $Ba_3ErRu_2O_9$, respectively, consistent with the magnetic transitions observed in dc and ac susceptibility measurements. In $Ba_3TbRu_2O_9$, the magnetic structure is characterized by a propagation vector, $k = (0, 0, 0)$, where Tb and Ru order ferromagnetically in the *ab* plane. Neighboring planes of Tb are coupled antiferromagnetically along the *c* direction as are neighboring planes of Ru, which leads to an AFM order between Tb and Ru as well. In contrast, the magnetic structure of $Ba_3ErRu_2O_9$ is characterized by $k = (0.5, 0, 0)$, with Er and Ru moments exhibiting a canted AFM ordering. Interestingly, the collinear (noncollinear) AFM order of Tb (Er) accompanied by the collinear (noncollinear) magnetic order of Ru in $Ba_3TbRu_2O_9$ ($Ba_3ErRu_2O_9$) along with the concurrent ordering of the rare earth and Ru in both compounds suggests a strong coupling between 4*f* and 4*d* electrons. Both compounds show weak magnetic ordering above T_N similar to that reported for $Ba_3HoRu_2O_9$. We have understood this intriguing feature by preparing a $Ba_3ErRu_2O_9$ sample with 3% excess RuO_2. Our analysis suggests that the weak magnetic ordering above T_N is strongly dependent on the excess RuO_2; however, and interestingly, the magnetic structure below T_N is robust against this RuO_2 surplus. Our detailed study provides insights into the magnetic ground states of these two compounds, thereby enhancing the understanding of magnetic ordering in this fascinating family.

DOI: 10.1103/pbtn-g5wz

I. INTRODUCTION

The rare earth (R) and $3d/4d/5d$ transition metal based magnetic compounds have attracted tremendous interest in the condensed matter community due to their fascinating physical properties like magnetoelectricity [1,2], multiferroicity [3,4], and exchange bias [5,6]. The competing $f-f$, $d-f$, and $d-d$ magnetic interactions in these compounds are responsible for these physical properties and also give rise to a rich diversity of complex magnetic ground states. Consequently, extensive investigations have been carried out to study the magnetic ordering of both rare earth and transition metals in these compounds. For instance, the $R_2Ru_2O_7$ exhibit two magnetic transitions corresponding to the independent magnetic ordering of R and Ru sublattices [7–9]. In contrast, in A_2RRuO_6 (A = Ca, Sr) [10,11] and $R_2Ir_2O_7$ [12–14], the magnetic order of R is induced by the internal field of Ru and Ir, respectively, below the Néel temperature (T_N). Moreover, in other f and d electron systems such as R_3RuO_7 (R = Tb, Nd) [15], both R and Ru sublattices order simultaneously below T_N, exhibiting ordered moment type behavior, which indicates a strong coupling between them. Recently, the interest in magnetic order has extended to another R and Ru (4*f*-4*d*) based family of compounds, $Ba_3RRu_2O_9$ (B*R*RuO), which shows exotic magnetic and electrical properties. Interestingly, some of the compounds of this family are also identified as geometrically frustrated systems [16].

The work on B*R*RuO compounds was pioneered by Doi and Hinatsu in the early 2000s [17]. These compounds (with R = La-Lu) crystallize in the hexagonal crystal structure (space group: $P6_3/mmc$) [Fig. 1(a)]. In this crystal structure, the R atom is coordinated by oxygen to form a RO_6 octahedron, while two distorted RuO_6 octahedra possess different Ru-O1 and Ru-O2 bond lengths and are face sharing, thus forming a Ru_2O_9 dimer. The geometry of the crystal structure facilitates R(Ru)-O2-Ru(R) and Ru-O1-Ru superexchange paths [Figs. 1(b) and 1(c)] which leads to the emergence

*Contact author: deepak1.phy@gmail.com

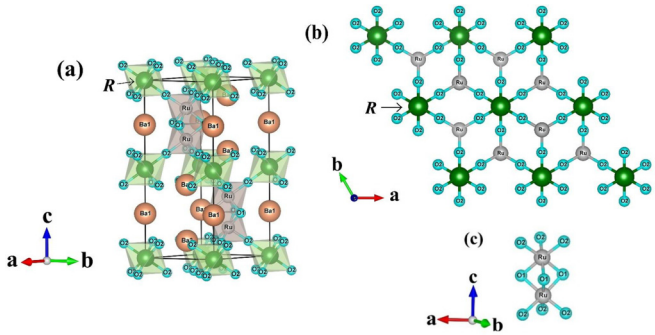

FIG. 1. (a) Hexagonal crystal structure of $Ba_3RRu_2O_9$ (B*R*RuO) compounds. Here Ba1 and Ba2 occupy $2b$ (0, 0, 1/4) and $4f$ (1/3, 2/3, z) Wyckoff positions, respectively, R at $2a$ (0, 0, 0), Ru at $4f$ (1/3, 2/3, z), O1 at $6h$ (x, $2x$, 1/4), and O2 at $12k$ (x, $2x$, z). (b,c) Different views of crystal structure showing R(Ru)-O2-Ru(R) and Ru-O1-Ru superexchange pathways in these compounds. Ba and O1 atoms in (b) are omitted for clarity.

of various intriguing and complex magnetic ground states ranging from ferromagnetic (FM) to antiferromagnetic (AFM) depending upon the R atom [17,18]. Despite these versatile magnetic ground states, only a few compounds of the B*R*RuO family have been investigated to date using neutron powder diffraction (NPD). For instance, Senn *et al.* solved the magnetic structure of BNdRuO using high-resolution NPD data measured at WISH, ISIS where they reported the Nd ordering in FM arrangement at 24 K followed by its spin canting with propagation vector, $k = (0, 0, 0)$ and FM Ru ordering in a Ru_2O_9 dimer coupled antiferromagnetically with the neighboring dimers below 18 K with $k = (0.5, 0, 0)$ [16]. This is in contrast with an earlier NPD study on BNdRuO by Doi *et al.* who reported only FM Nd ordering below 24 K [18]. Similar to BNdRuO, NPD studies of Doi *et al.* [19,20] at 2 K on BTbRuO showed only collinear AFM Tb ordering without giving any information on a possible Ru ordering. Very recently, Kushwaha *et al.* [21] reported an entirely different magnetic structure for BTbRuO consisting of a canted AFM Tb ordering in the bc plane and a collinear AFM Ru ordering along the b direction. They also reported the magnetic space group of this compound as $P6_3'/m'm'c$. However, this space group does not correspond to their reported magnetic structure. In fact, this space group allows only c components of the magnetic moments. Therefore, the exact description of the magnetic structure of this compound is still lacking. In the present study, we have solved the magnetic structure of BTbRuO by performing high-intensity NPD measurements. Basu *et al.* [22] reported a simultaneous magnetic ordering of both Ho and Ru in BHoRuO at $\sim$50 K (T_{N1}) with $k_1 = (0.5, 0, 0)$, a temperature well above the magnetic ordering temperature $\sim$10 K (T_{N2}) determined from dc susceptibility data. Below 10 K, the magnetic structure of BHoRuO was characterized by two propagation vectors, $k_1 = (0.5, 0, 0)$ and $k_2 = (0.25, 0.25, 0)$. Thus the magnetic structure study of BHoRuO has generated significant additional interest in investigating the magnetic structure of other B*R*RuO compounds with a heavy R atom. The present work also involves the determination of the unprecedented magnetic structure of BErRuO.

Our high-intensity NPD data analysis of BTbRuO and BErRuO reveals AFM ground states in both compounds, consistent with the magnetic transitions observed in the dc and ac susceptibility studies. The AFM ground state in BTbRuO is characterized by $k = (0, 0, 0)$ with collinear AFM ordering of both Tb and Ru spins at variance with the results reported by Kushwaha *et al.* [21]. While in BErRuO, the AFM ground state is characterized by $k = (0.5, 0, 0)$ with a canted or noncollinear AFM ordering of Er and Ru spins. Notably, the collinear and noncollinear magnetic structures along with the simultaneous magnetic ordering of both sublattices in both compounds demonstrates a strong $4f$-$4d$ coupling.

II. EXPERIMENTAL DETAILS

Polycrystalline samples of $Ba_3RRu_2O_9$ (R = Tb, Er) were prepared by the conventional solid-state reaction method. Stoichiometric amounts of high-purity starting chemicals $BaCO_3$, RuO_2, and either Tb_4O_7 or Er_2O_3 (depending upon the sample) were weighed and mixed in an agate mortar with a pestle. The mixtures were heated at 900 °C and 1200 °C for 12 h each with intermediate grinding. After that, the mixtures were ground, pelletized, and heated at 1300 °C and 1350 °C for 24–48 h with several intermediate grindings and repelletization. The single-phase nature of the compounds was checked by recording the (Cu $K\alpha$) x-ray diffraction pattern at room temperature using a Bruker D2 phaser. The dc magnetization (M versus T and M versus H) measurements were performed on a Quantum Design Physical Property Measurement System (QD-PPMS) DynaCool 14. The dc magnetization (M versus T) curves were recorded between 1.8 and 380 K under various applied magnetic fields in zero field cooled (ZFC) and field cooled (FC) modes. The hysteresis loops (M versus H) were recorded in the magnetic-field range of $\pm$70 kOe at various temperatures. The ac susceptibility of both compounds was measured over a 1.8–50 K temperature range under various frequencies by applying an excitation field of 5 Oe using the ACMS option of QD-PPMS.

Neutron powder diffraction (NPD) experiments were carried out at various temperatures on the high-intensity D20 diffractometer, $\lambda = 2.42$ Å, at the Institut Laue-Langevin (ILL), Grenoble, France. For both compounds, high-statistic NPD data were collected for 2 h at some selected temperatures while additional temperature-dependent patterns were collected using a ramp speed of 0.1 K every 40 s with each data collected for 15 min. All x-ray and neutron diffraction patterns are plotted as a function of magnitude of momentum transfer, $Q = 4\pi \sin\theta/\lambda$, where θ is the Bragg angle and λ is the wavelength of the radiation used. Diffraction patterns were analyzed by the Rietveld refinement technique [23] using FULLPROF software [24]. The magnetic structures were solved using magnetic symmetry analysis and magnetic space group analysis using the BASIREPS program included in the FULLPROF software [24] and the MAXMAGN program of the Bilbao Crystallographic Server [25], respectively.

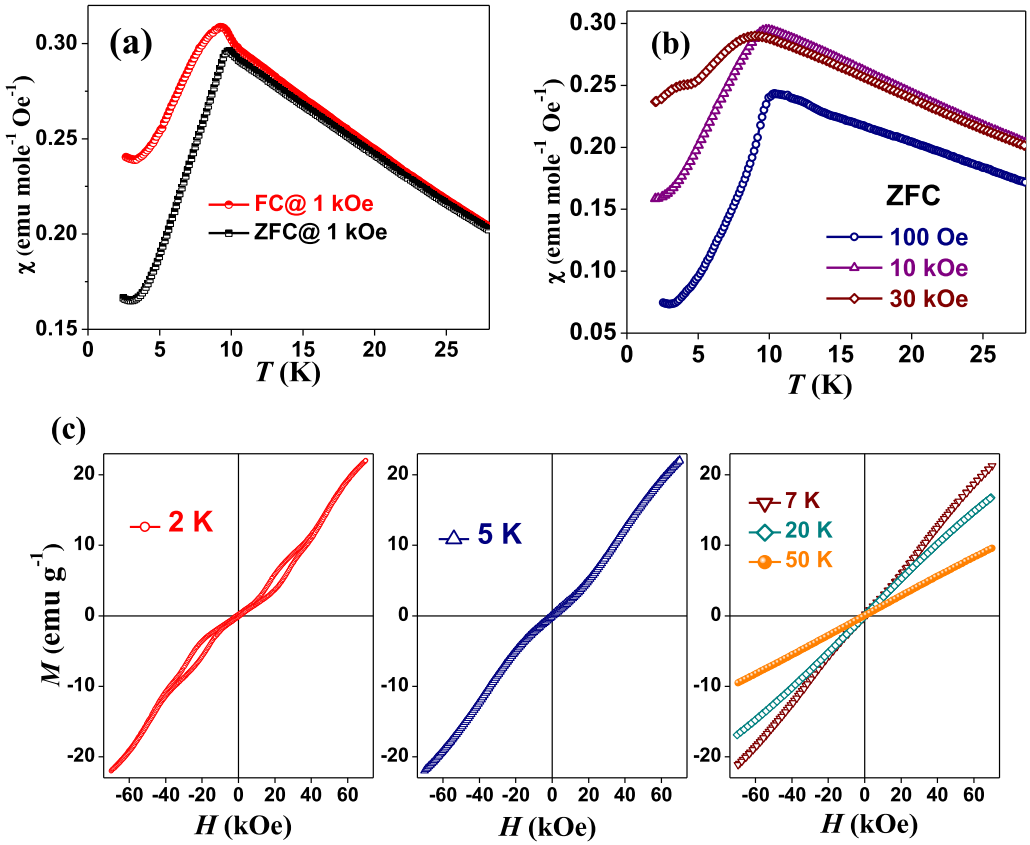

FIG. 2. (a) Temperature dependence of dc susceptibility, χ ($= M/H$), under $H = 1$ kOe in ZFC and FC modes for the BTbRuO compound. (b) ZFC χ vs T curves under different magnetic fields. (c) M-H hysteresis loops at selected temperatures.

III. RESULTS

A. X-ray diffraction

Rietveld refinement results of the x-ray diffraction (XRD) (Cu $K\alpha$) of both compounds are presented in Fig. S1 in the Supplemental Material (SM) [26]. All Bragg peaks are indexed in the hexagonal crystal structure (space group: $P6_3/mmc$) inferring the single phase of both compounds. We could not see any impurity phase from the XRD data; however, Rietveld refinement on the NPD reveals ∼0.6 wt % Er_2O_3 impurity phase in BErRuO (NPD results are presented later). The derived lattice constants, $a(= b) = 5.841(4)$ Å, $c = 14.435(2)$ Å for BTbRuO and $a(= b) = 5.877(1)$ Å, $c = 14.477(1)$ Å for BErRuO, are in good agreement with the literature [17]. The crystal structure is shown in Fig. 1. Structural parameters for both compounds are listed in Table S1 in the SM [26] and are also in good agreement with the literature values [17]. The structural parameters derived from the Rietveld refinement of 1.6 K NPD data are also included in Table S1 (NPD analysis is presented later).

B. dc and ac susceptibility

Figure 2(a) shows the dc susceptibility (χ) of BTbRuO as a function of temperature (T) under a magnetic field (H) of 1 kOe in FC and ZFC modes. For clarity, only the low-temperature region is shown. The complete data are shown in Fig. S2(a) in the SM [26]. A sharp decrease in the magnetic susceptibility at ∼9.8 K is clearly evident from the data, indicating an AFM transition in the compound, consistent with the literature [19]. A similar magnetic behavior is also observed for $H = 100$ Oe and 10 kOe ZFC susceptibility data [Fig. 2(b)]. However, for higher $H = 30$ kOe, the AFM transition becomes broad and shifts to a slightly lower temperature. Additionally, a hump is observed at low temperatures below 5 K, which is well consistent with the observation of a double hysteresis-loop-like behavior around this H value [see Fig. 2(c); 2 K data]. This may be due to some domain dynamics in the sample at high fields. With increasing temperature, the double hysteresis loop feature diminishes, and a linear hysteresis curve is observed in the paramagnetic state [see second and third panels of Fig. 2(c)].

The ZFC and FC χ versus T curves of the BErRuO compound under $H = 1$ kOe are presented in Fig. 3(a) where two magnetic transitions, a sharp and a broader one at lower T, are evident. For clarity, only the low-temperature region is shown. The complete χ curves over the temperature range of 1.8–380 K are shown in Fig. S2(b) in the SM [26]. The derivative curve shows two peaks at ∼3.6 and 6 K [Fig. 3(a), right y axis] corresponding to these magnetic transitions. The sharp peak at ∼6 K corresponds to an AFM transition in the compound. For higher H, the AFM transition temperature shifts to the lower temperature while the broad anomaly disappears [Fig. 3(b)]. The M versus H hysteresis loops at various temperatures are displayed in Fig. 3(c). It is evident that these hysteresis loops look different than those of BTbRuO [Fig. 2(c)], suggesting

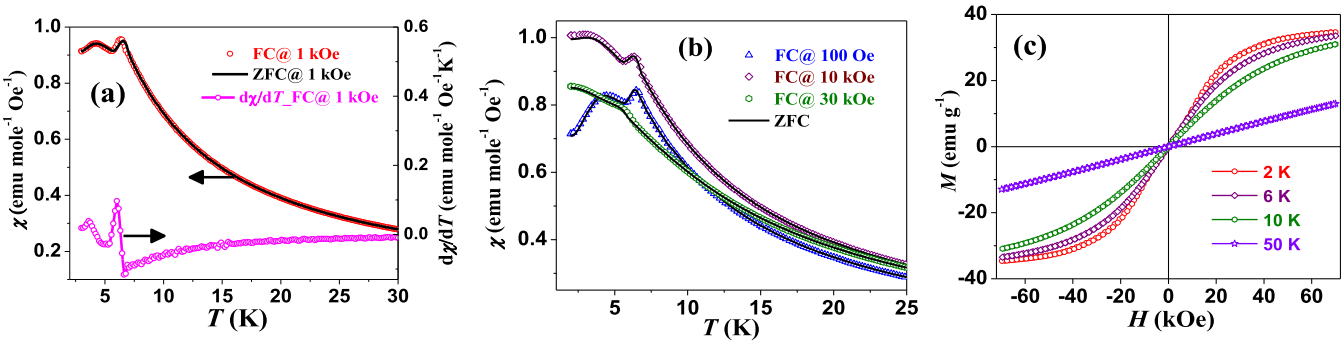

FIG. 3. FC and ZFC χ vs T curves of BErRuO under (a) $H = 1$ kOe and (b) various other magnetic fields. (c) M vs H hystersis loops at selected temperatures. The right axis in (a) represents the FC dχ/dT curve under $H = 1$ kOe, showing two magnetic transitions at ∼3.6 and 6 K.

different domain dynamics with magnetic field in two compounds.

Ac susceptibility measurements performed on both compounds, as a function of temperature at frequencies ranging from 111 to 9999 Hz, are shown in Fig. 4. The magnetic transitions deduced from these measurements are well consistent with the corresponding ones observed in the dc susceptibility study. It is also evident that BErRuO [Fig. 4(b)] does not show any noticeable frequency dependence while the magnetic transition at ∼9.7 K in BTbRuO (close to 9.8 K in dc susceptibility) under 111 Hz data shifts to slightly higher temperature ∼9.9 K with increasing frequency [Fig. 4(a)], suggesting a possible very minor spin-glass phase in the compound.

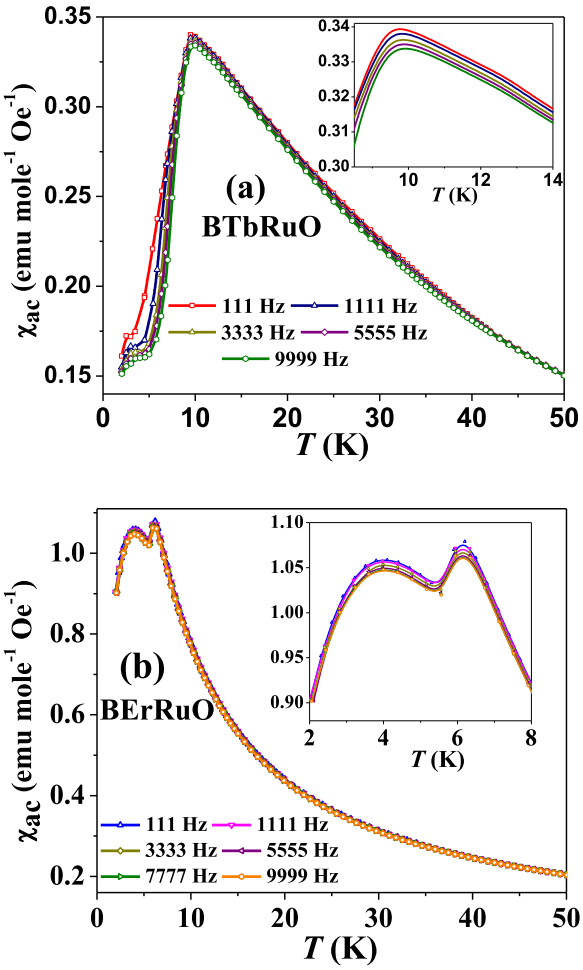

FIG. 4. Real part of the ac susceptibility (χ_{ac}) as a function of temperature (T) for (a) BTbRuO and (b) BErRuO compounds under various frequencies. Zoomed-in view of the data near the magnetic transitions is shown in their corresponding insets.

C. Magnetic ground state and magnetic structure

1. $Ba_3TbRu_2O_9$ *(BTbRuO)*

Figure 5(a) shows the high-intensity NPD patterns of BTbRuO at some selected temperatures. Below the magnetic ordering temperature, T_N ∼9.8 K, several Bragg peaks gain in intensity, indicating their magnetic origin [see 1.6–15 K difference NPD data in Fig. 5(b)]. All these reflections can be indexed with the propagation vector, $k = (0, 0, 0)$. The integrated intensities of some of these Bragg peaks are plotted as a function of temperature in Fig. 5(c). The observed enhancement in the integrated intensities indicates the growth of ordered magnetic moments.

The Rietveld refinement of the NPD data measured at 15 K ($T > T_N$) gives good agreement between the experimental and calculated patterns assuming the hexagonal $P6_3/mmc$ crystal structure [Fig. 6(a)]. To solve the magnetic structure of the compound, symmetry analysis was carried out using the BASIREPS program considering the propagation vector, $k = (0, 0, 0)$. The program gives four magnetic irreducible representations (IRs) corresponding to the Tb site with one or two basis vectors (BVs), and eight IRs corresponding to the Ru site having one or two BVs as well. The IRs and BVs for Tb and Ru sites are listed in Tables I and II, respectively. Rietveld refinement at all temperatures below T_N reveals that IR4 is the best magnetic model to account for the intensities of all magnetic Bragg peaks; for instance, see Fig. 6(b) for the 1.6 K NPD data. The derived magnetic moments at 1.6 K for Tb and Ru sites are $m_z = 6.52(2)\,\mu_B$ and $m_z = -0.43(3)\,\mu_B$, respectively. Since the derived Ru moment is small, therefore, to check the reliability of such a small moment, we have also refined the high-statistics NPD difference data, 1.6–15 K and 8–15 K. For this analysis, the scale factor, derived from the Rietveld refinement of the high-statistics NPD data collected in the paramagnetic state at 15 K, was kept fixed. The

TABLE I. Irreducible representations (IRs) and basis vectors (BVs) of the space group $P6_3/mmc$ for the Tb site (0, 0, 0) for BTbRuO under the propagation vector, $k = (0, 0, 0)$. The last two columns on the right contain the correspondence to the notation as used in [21].

		x, y, z			$-x, -y, z+1/2$				
IRs	BVs	m_x	m_y	m_z	m_x	m_y	m_z	From Ref. [21]	
IR2	BV1	0	0	1	0	0	1	ψ_1	Γ_3
IR4	BV1	0	0	1	0	0	−1	ψ_2	Γ_7
IR5	BV1	1	0	0	−1	0	0	ψ_5	Γ_{11}
	BV2	0.5	1	0	−0.5	−1	0	ψ_6	
IR6	BV1	0.5	1	0	0.5	1	0	ψ_4	Γ_9
	BV2	−1	0	0	−1	0	0	ψ_3	

resulting Rietveld refinements for the 1.6–15 K data are shown in Figs. 6(c) and 6(d). Assuming only a magnetic moment on the Tb site [$m_z = 6.59(1)\,\mu_B$] as postulated by Doi *et al.* [19,20] a magnetic *R* factor (R_{mag}) of 4.8 was achieved [Fig. 6(d)]. A better Rietveld refinement with a lower goodness of fit parameter ($R_{mag} = 2.9$) was achieved by considering again magnetic moments on both sites [$m_z = 6.58(1)\,\mu_B$ for Tb and $m_z = -0.35(1)\,\mu_B$ for Ru] in the Rietveld analysis [Fig. 6(c)], further supporting the existence of an ordered Ru magnetic moment in the compound. The small value of the Ru magnetic moment could be the reason that it was not determined in the previous NPD studies of BTbRuO by Doi *et al.* [19,20]. The derived magnetic structure of BTbRuO is shown in Fig. 7(a). Both Tb and Ru moments are coupled ferromagnetically in the *ab* plane, and these planes are coupled antiferromagnetically along the *c* axis. Moreover, a collinear AFM Ru ordering in the Ru_2O_9 dimers becomes apparent. The Rietveld derived total Tb and Ru moments at all temperatures are plotted in Fig. 7(b). Both moments are nicely following an order parameter type temperature dependence.

This magnetic structure is well consistent with the one determined by Doi *et al.* [19,20] as far as it concerns the Tb ordering. On the other hand, very recently, the magnetic structure of this compound reported by Kushwaha *et al.* [21] is entirely different than the magnetic structure derived by us [Fig. 7(a)] and Doi *et al.* [19,20]. Kushwaha *et al.* [21] reported a magnetic structure consisting of canted AFM Tb ordering in the *bc* plane and collinear AFM Ru ordering along the *b* axis. They used a combination of different IRs $\Gamma_{11}(\psi_5)$ for Ru and $\Gamma_7(\psi_2)$, $\Gamma_{11}(\psi_5)$ for Tb, using the notations as given in their Tables S1 and S2 as derived from the SARAh program [27], to fit their NPD data. However, we notice that there is no ψ_5 basis vector corresponding to Γ_{11} for Ru. It should be either ψ_9 *or* ψ_{10} according to their reported basis vector list. Since according to them, the Ru moment is along the *b* axis, it should be ψ_9. To check their model, we have performed Rietveld refinement on our high-statistics, 1.6–15 K NPD data by considering their model, and the results are shown in Fig. 8. It can be seen that first the high-intensity magnetic Bragg peaks (101)(003) at $Q = 1.32\,\text{Å}^{-1}$ are not correctly fitted and, secondly, their magnetic model generates two extra Bragg peaks at $Q = 1.52\,\text{Å}^{-1}$ (shown enlarged view) and $2.14\,\text{Å}^{-1}$ (marked by asterisk) which corresponds to (102) and (104)(110) reflections, respectively, in the present NPD data [see Fig. 5(a)]. It should be noted that these Bragg peaks do not have any magnetic contribution in our data, at least within the detection limit of the instrument used. According to the reported time of flight NPD data shown in Fig. 2(a) of Ref. [21] and its text description, Bragg peaks (101) and (103) have only a magnetic contribution below $T_N = 9.5\,\text{K}$ (see Figs. 2(b)–2(d) of Ref. [21]). These results are consistent with the present NPD data. However, the time of flight NPD data presented in Fig. 3(a) of Ref. [21] show that the (102) Bragg peak has a very small magnetic

TABLE II. Irreducible representations (IRs) and basis vectors (BVs) of the space group $P6_3/mmc$ for the Ru site (1/3, 2/3, *z*) for BTbRuO under the propagation vector, $k = (0, 0, 0)$. The last two columns on the right contain the correspondence to the notation as used in [21].

		x, y, z			$-x, -y, z+1/2$			$x-y, -y, -z$			$x, x-y, -z+1/2$				
IRs	BVs	m_x	m_y	m_z	m_x	m_y	m_z	m_x	m_y	m_z	m_x	m_y	m_z	From Ref. [21]	
IR2	BV1	0	0	1	0	0	1	0	0	1	0	0	1	ψ_2	Γ_3
IR4	BV1	0	0	1	0	0	−1	0	0	1	0	0	−1	ψ_4	Γ_7
IR5	BV1	1	0	0	−1	0	0	1	0	0	−1	0	0	ψ_9	Γ_{11}
	BV2	0.5	1	0	−0.5	−1	0	0.5	1	0	−0.5	−1	0	ψ_{10}	
IR6	BV1	0.5	1	0	0.5	1	0	0.5	1	0	0.5	1	0	ψ_5	Γ_9
	BV2	−1	0	0	−1	0	0	−1	0	0	−1	0	0	ψ_6	
IR7	BV1	0	0	1	0	0	1	0	0	−1	0	0	−1	ψ_1	Γ_2
IR9	BV1	0	0	1	0	0	−1	0	0	−1	0	0	1	ψ_3	Γ_6
IR11	BV1	1	0.5	0	−1	−0.5	0	−1	−0.5	0	1	0.5	0	ψ_{11}	Γ_{12}
	BV2	0	−1	0	0	1	0	0	1	0	0	−1	0	ψ_{12}	
IR12	BV1	1	0	0	1	0	0	−1	0	0	−1	0	0	ψ_7	Γ_{10}
	BV2	0.5	1	0	0.5	1	0	−0.5	−1	0	−0.5	−1	0	ψ_8	

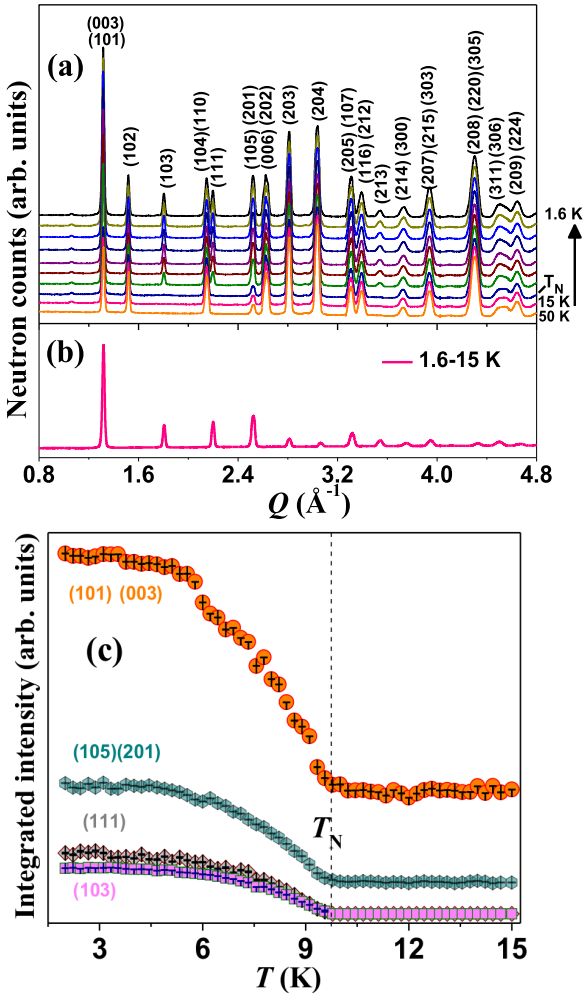

FIG. 5. (a) NPD patterns at some selected temperatures collected at the high-intensity D20 diffractometer, ILL. The patterns are shifted vertically upward for better visualization of the magnetic Bragg peaks. All Bragg peaks are indexed by *hkl* values. (b) The 1.6–15 K difference NPD data showing only magnetic Bragg peaks. (c) Thermal variation of the integrated intensity of some of the magnetic Bragg peaks. Vertical dotted line corresponds to the T_N of the compound.

contribution at both 2 K (below T_N) and 20 K (above T_N) as compared to the 100 K data, which is contrary to T_N being at 9.5 K and contradictory with the statement mentioned in the text that no other magnetic Bragg reflections were seen at low temperature in the Q range between 1 and 2 Å^{-1} where the (102) reflection should appear. Different intensities of Bragg peaks at two temperatures above T_N can be seen as well in Fig. 3(a) of Ref. [21] for other Bragg peaks including (101), which is not in agreement either with their NPD data presented in Fig. 2, according to which this Bragg peak has no magnetic contribution above T_N. To check this issue in the present NPD data, we have plotted the NPD data at 15 K (above T_N) and 50 K (well above T_N) in the paramagnetic state in Fig. S3 in the SM [26]. Both data entirely overlap, suggesting no magnetic contribution in the paramagnetic state, as should be the case. Therefore, we believe that this discrepancy in the magnetic structure models presented here and in Ref. [21] arises due to different NPD data quality and/or perhaps to the normalization issue. Based on the above arguments, the present study rules out the magnetic structure model reported in Ref. [21]. As expected, we could get a good Rietveld fit using only $\Gamma_7(\psi_2)$ for Tb and $\Gamma_7(\psi_4)$ for the Ru sites (Fig. S4(a) in the SM [26]), and the derived magnetic structure exactly matches that derived from the basis vectors formalism using BASIREPS (IR4, BV1). Apart from the fact that the solution proposed in [21] leads to magnetic peaks not existing in our high-statistics difference data, one has to note here that the mixing of two IRs is in contradiction to Landau's theory for a second-order transition, according to which only one IR should be active. Further, to make our argument stronger, we have also fitted the NPD data using magnetic space group formalism. Using the program MAXMAGN of the Bilbao Crystallographic Server, one can derive, for the parent paramagnetic $P6_3/mmc$ space group with propagation vector $k = (0, 0, 0)$, eight maximal magnetic space groups which are listed as follows: $P6_3/m'm'c'$, $P6_3/mm'c'$, $P6'_3/m'mc'$, $P6'_3/m'm'c$, $P6'_3/mmc'$, $P6'_3/mm'c$, $P6_3/m'mc$, and $P6_3/mmc$ having numbers 194.271, 194.270, 194.269, 194.268, 194.267, 194.266, 194.265, and 194.263, respectively. Out of these magnetic space groups, there are no Tb and Ru magnetic moments associated with $P6'_3/m'mc'$(194.269), $P6'_3/mmc'$(194.267), $P6_3/m'mc$(194.265), and $P6_3/mmc$ (194.263). For $P6_3/m'm'c'$ (194.271) and $P6'_3/mm'c$ (194.266), the only allowed magnetic moment component is a z component of Ru. This cannot be the magnetic structure solution because Ru alone cannot account for the strong magnetic contribution in the NPD pattern. In the $P6_3/mm'c'$ (194.270) and $P6'_3/m'm'c$ (194.268) magnetic space groups, only z components of the magnetic moments of both Tb and Ru sites are allowed. We could get a good Rietveld refinement of our NPD data by considering $P6'_3/m'm'c$ (194.268) (see Fig. S4(b) in the SM [26]). It is interesting to note that the derived magnetic structure is again exactly the same as that derived using basis vector formalism from BASIREPS (IR4, BV1) and SARAh [$\Gamma_7(\psi_2)$ for Tb and $\Gamma_7(\psi_4)$ for Ru]. Further, Kushwaha *et al.* [21] also reported a very large Ru moment of 1.96 μ_B at 2 K. We would like to point out that if such a large Ru moment were present in BTbRuO compound, then it would have been detected by Doi *et al.* [19,20] in their studies on the same compound as they detected a Nd moment of 1.65 μ_B in BNdRuO [18]. A small Ru moment of $\sim$0.6 μ_B was reported by Senn *et al.* [16] in BNdRuO using NPD measurements at the WISH diffractometer, ISIS, indicating that the Ru moment in these B*R*RuO compounds seems to be small.

In brief, our NPD study has provided the magnetic ground state of the BTbRuO compound involving the collinear AFM Tb and hidden Ru magnetic ordering aligned along the c axis. The magnetic structure is well consistent with both the representation analysis and the magnetic space group formalisms. Below, we present the magnetic structure results of the BErRuO compound.

2. $Ba_3ErRu_2O_9$ *(BErRuO)*

To investigate the magnetic structure of the BErRuO compound, we performed NPD experiments in the temperature

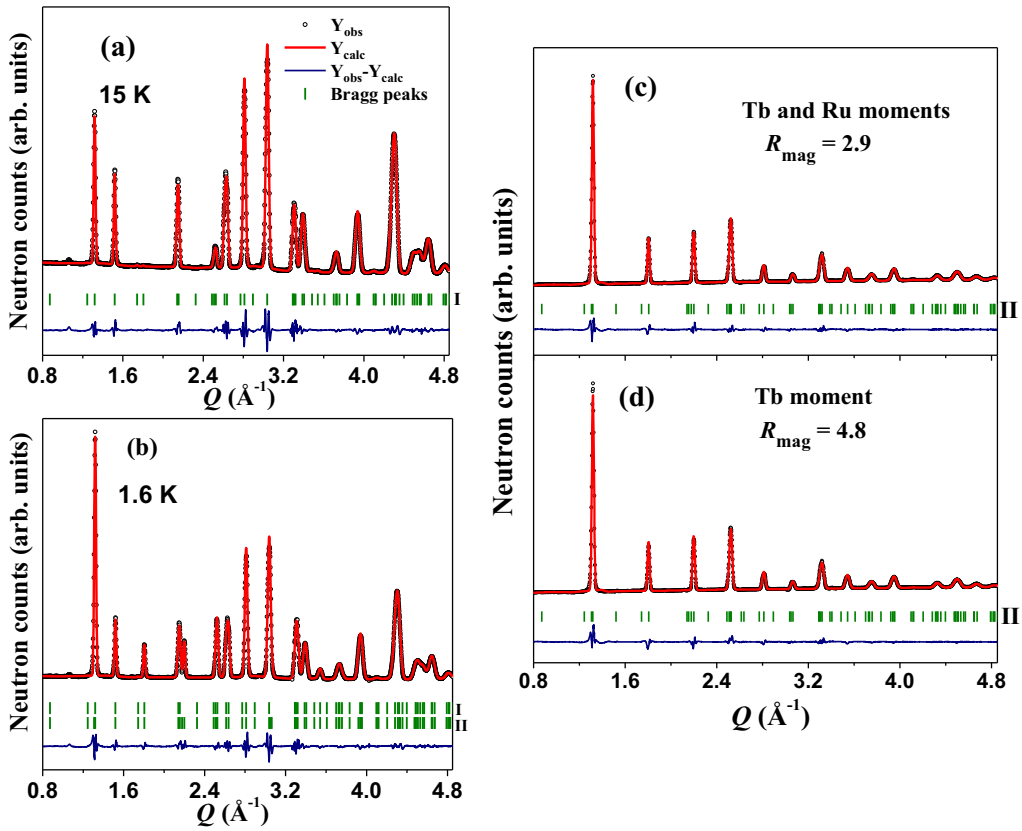

FIG. 6. Experimentally observed (open black symbols) and calculated (solid red line) NPD data at (a) 15 K, (b) 1.6 K, and [(c),(d)] 1.6–15 K. The difference of two data is shown by a navy blue line. Vertical ticks, I and II, represent the nuclear and magnetic Bragg peaks, respectively. Rietveld refinement shown in [(c),(d)] is carried out on the 1.6–15 K difference NPD data by considering (c) both Tb and Ru moments and (d) only the Tb moment. Other details are given in the text.

range of 1.6–50 K again using the high-intensity D20 diffractometer. Figure 9(a) shows NPD patterns at some selected temperatures. On comparing the NPD data of BTbRuO and BErRuO compounds below their T_N, we could notice that the BErRuO shows various magnetic Bragg peaks at different scattering vectors (Q), indicating a different and more complex magnetic structure than BTbRuO. We could index all magnetic Bragg peaks of BErRuO with the propagation vector, $k = (0.5, 0, 0)$. It is interesting to note that not all magnetic Bragg peaks disappear at $T_N \sim 6$ K. Weak intensity is left on the magnetic reflections (0.5 0 2), (0.5 −1 3), (0.5 1 2), and (0.5 −2 −2) at $Q = 1.06$, 1.69, 1.85, and 2.39 Å^{-1}, respectively, as can be seen in Fig. 9(b), which corresponds to a difference pattern between the high-statistics

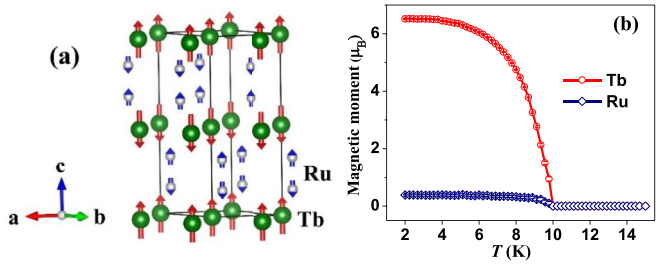

FIG. 7. (a) Magnetic structure of BTbRuO compound. Magnetic moments corresponding to an enlarged magnetic unit cell are shown for better visualization of the magnetic interactions in the *ab* plane. (b) Thermal variation of total Tb and Ru magnetic moments.

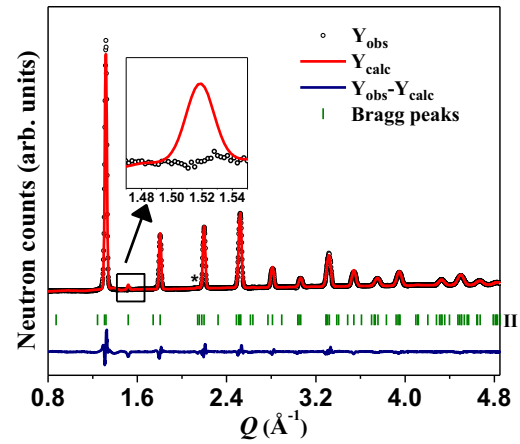

FIG. 8. Rietveld refined 1.6–15 K NPD data using a magnetic model consisting of $\Gamma_7(\psi_2)$, $\Gamma_{11}(\psi_5)$ for Tb and $\Gamma_{11}(\psi_9)$ for Ru, as reported in Ref. [21]. These representations follow a notation as defined using the SARAh program [27]. Two extra Bragg peaks at $Q = 1.52$ Å^{-1} (shown enlarged view) and 2.14 Å^{-1} (marked by *) are generated by the model as proposed by Kushwaha *et al.* [21].

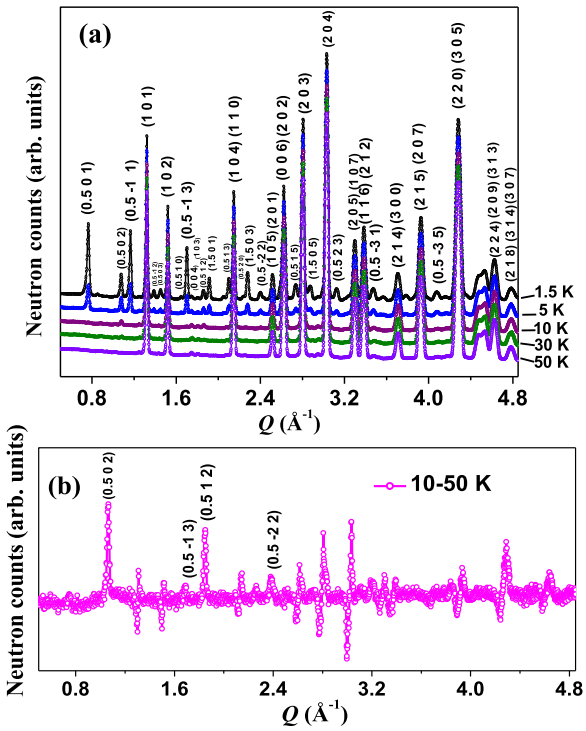

FIG. 9. (a) NPD patterns of the BErRuO compound at some selected temperatures. The patterns are vertically shifted for better clarity. All Bragg peaks are indexed by *hkl* values. (b) The 10–50 K difference NPD data showing the presence of magnetic Bragg peaks persisting above T_N ($\sim$6 K). The up and down features in the 10–50 K data are attributed to the different lattice constants at these temperatures.

NPD data taken at 10 and 50 K. Using the shorter scans, the temperature dependence of the different magnetic peaks could be followed in more detail. Figures 10(a) and 10(b) show the disappearance of the majority of the magnetic reflections at T_N while Figs. 10(c)–10(f) show those which persist above T_N $\sim$6 K. The magnetic Bragg peak (0.5 0 2) persists up to $\sim$40 K [Fig. 10(c)], while (0.5 1 2), (0.5 −1 3), and (0.5 −2 −2) disappear at the background level of the short NPD scans at $\sim$26, $\sim$7.5, and $\sim$6.7 K, respectively [Figs. 10(d)–10(f)]. The presence of (0.5 −1 3), (0.5 −2 −2) and (0.5 1 2) Bragg peaks above these temperatures is, however, evident from the long scan 10–50 K [Fig. 9(b)] and 30–50 K (not shown) difference NPD data. The different temperatures, above which these weak magnetic reflections are no longer observed, are due to the different counting time for these NPD data which directly affects the magnetic signal to noise ratio of these Bragg peaks. The (0.5 0 2) and (0.5 1 2) magnetic Bragg peaks show a small increase in intensity down to T_N $\sim$6 K; however, below this temperature, a sharp increase in intensity can be noted. Thus, these results indicate that the magnetic ordering sets in the BErRuO compound well above T_N, as determined from dc and ac susceptibility measurements.

Figure 11(a) shows the Rietveld refined NPD data in the paramagnetic state at 50 K confirming the hexagonal crystal structure with $P6_3/mmc$ space group, consistent with the x-ray diffraction study. The Rietveld refinement also infers $\sim$0.6 wt% Er_2O_3 impurity phase in the compound. To analyze the magnetic Bragg peaks for determining the magnetic structure, symmetry analysis was carried out considering the $P6_3/mmc$ space group and propagation vector, $k = (0.5,\ 0,\ 0)$, using the BASIREPS program. The derived IRs

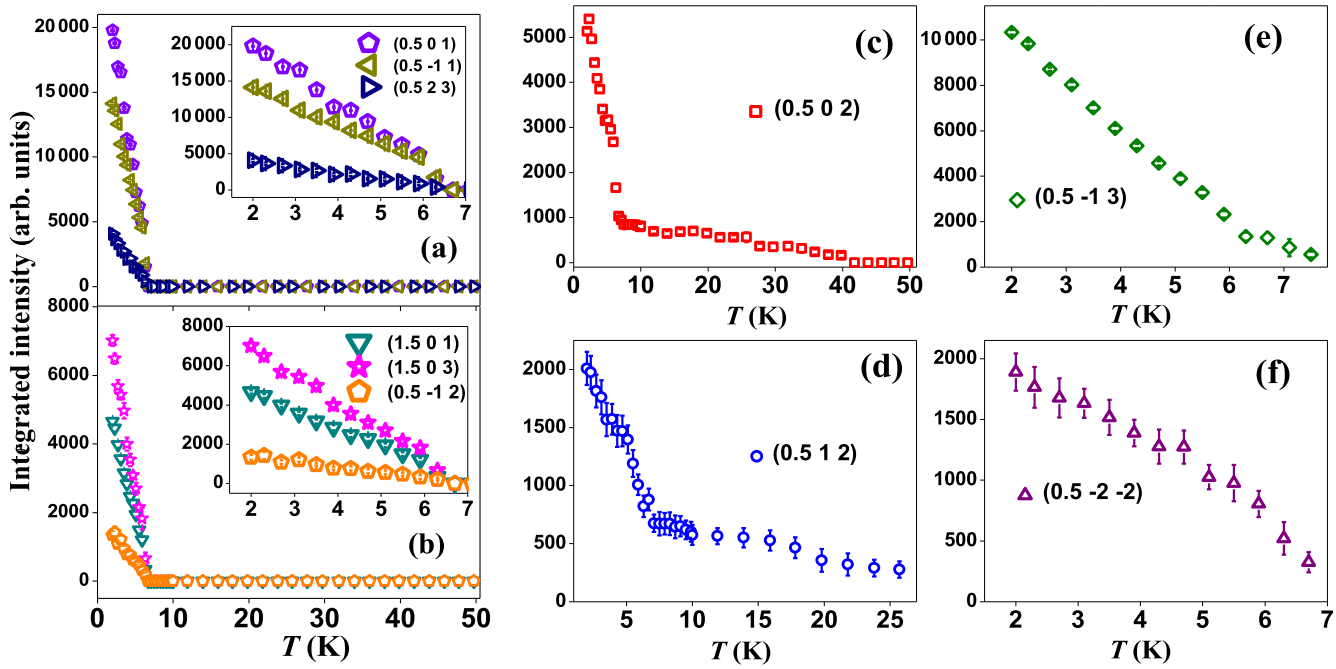

FIG. 10. (a)–(f) Thermal variation of integrated intensity of magnetic Bragg peaks as determined from the shorter scans NPD data. The zoomed-in views of the magnetic Bragg peak intensity shown in the main panels of [(a),(b)] are presented in their corresponding insets. These Bragg peaks exist up to T_N ($\sim$6 K), in contrast to other magnetic Bragg peaks shown in [(c),(d)]. The magnetic Bragg peaks shown in [(e),(f)] also perisist well above T_N, as evident from the high-statistics difference NPD data displayed in Fig. 9(b). (For details, see main text).

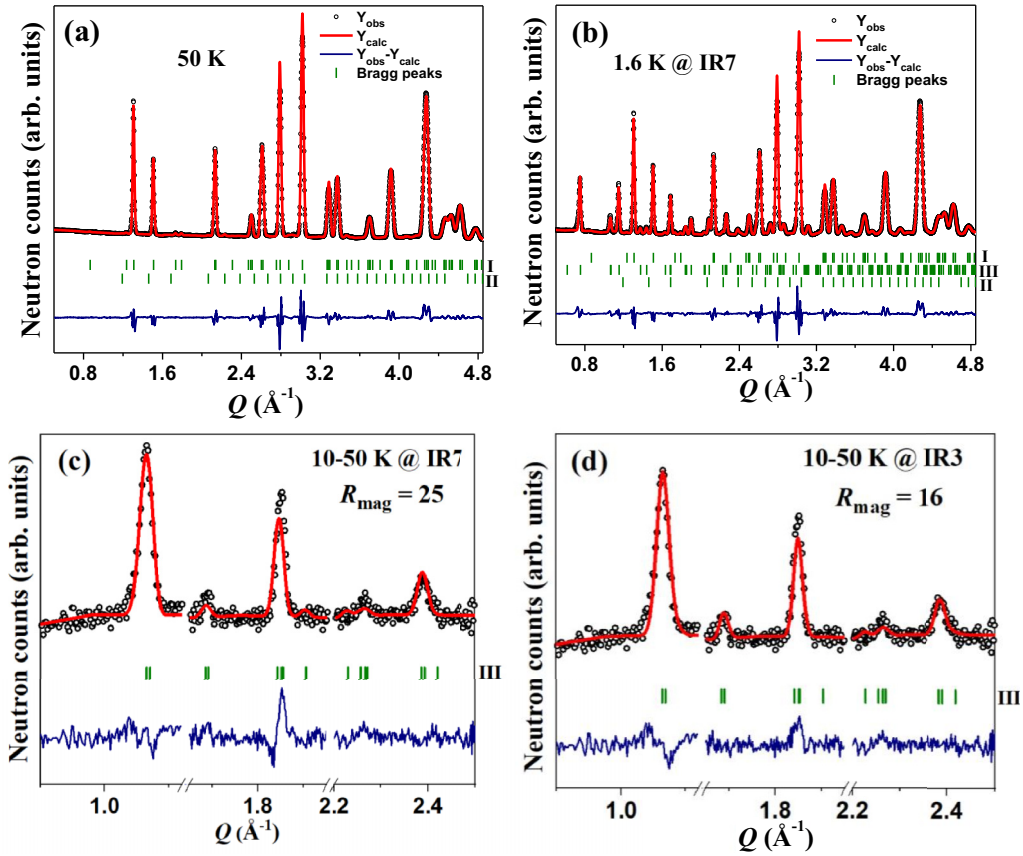

FIG. 11. Experimentally observed (open black symbols) and Rietveld refined (solid red line) NPD patterns at (a) 50 K, (b) 1.6 K, and [(c),(d)] 10–50 K. The difference between these two data is shown at the bottom by a navy blue line. The vertical (olive colored) marks I and III correspond to nuclear and magnetic Bragg reflections of the BErRuO (main phase) compound, respectively, while II represents the nuclear reflections of Er_2O_3 (impurity phase). The details of the IR7 and IR3 fitted models are given in the text.

and BVs for Er and Ru sites are listed in Tables III and IV, respectively. Symmetry analysis gives four and eight IRs for Er and Ru sites, respectively. We have tried all IRs in our Rietveld refinement, and we could get very good agreement between the experimental and calculated NPD data by considering IR7 [magnetic space group P_Cbcn (No. 60.431)] for both sites below T_N; the corresponding Rietveld refinement at 1.6 K is shown in Fig. 11(b). The refined Er and Ru magnetic moments at 1.6 K are $m_{ab}^{Er} = 2.48(4)\,\mu_B$, $m_c^{Er} = 4.63(2)\,\mu_B$ and $m_{ab}^{Ru} = -0.41(1)\,\mu_B$, $m_c^{Ru} = -0.50(1)\,\mu_B$ with their total moments $5.1(1)\,\mu_B$ and $0.61(2)\,\mu_B$, respectively. As mentioned earlier, the Bragg peaks viz., (0.5 0 2), (0.5 −1 3), (0.5 1 2), (0.5 −2 −2) at $Q = 1.06$, 1.69, 1.85, and 2.39 Å^{-1}, respectively, persist above $T_N \sim 6$ K, so now we focus on the NPD data analysis of the compound above T_N. Since these are weak magnetic Bragg peaks in comparison to those below T_N, the analysis uses the difference NPD data. Interestingly, we could get a better Rietveld refinement by considering the IR3 model, corresponding to magnetic space group P_Bnma (No. 62.454), with a lower goodness of fit parameter ($R_{mag} = 16$) [Fig. 11(d)] than the IR7 model with $R_{mag} = 25$ [Fig. 11(c)]. This indicates a change of magnetic structure across T_N. The refined Er and Ru magnetic moments are $m_{ab}^{Er} = 0.32(1)\,\mu_B$, $m_c^{Er} = 0.75(3)\,\mu_B$ and

TABLE III. Irreducible representations (IRs) and basis vectors (BVs) of the space group $P6_3/mmc$ for the Er site for BErRuO under the propagation vector, $k = (0.5,\ 0,\ 0)$.

		x, y, z			$-x, -y, z + 1/2$		
IRs	BVs	m_x	m_y	m_z	m_x	m_y	m_z
IR1	BV1	0	−1	0	0	1	0
IR3	BV1	1	0.5	0	0	0	1
	BV2	−1	−0.5	0	0	0	1
IR5	BV1	0	−1	0	0	−1	0
IR7	BV1	1	0.5	0	0	0	1
	BV2	1	0.5	0	0	0	−1

TABLE IV. Irreducible representations (IRs) and basis vectors (BVs) of the space group $P6_3/mmc$ for the Ru site (1/3, 2/3, z) for BErRuO under the propagation vector, $k = (0.5,\ 0,\ 0)$.

		x, y, z			$-x, -y, z+1/2$			$-x, -x+y, -z$			$x, x-y, -z+1/2$		
IRs	BVs	m_x	m_y	m_z	m_x	m_y	m_z	m_x	m_y	m_z	m_x	m_y	m_z
IR1	BV1	0	−1	0	0	1	0	0	−1	0	0	1	0
IR2	BV1	1	0.5	0	−1	−0.5	0	−1	−0.5	0	1	0.5	0
	BV2	0	0	1	0	0	1	0	0	−1	0	0	−1
IR3	BV1	1	0.5	0	−1	−0.5	0	1	0.5	0	−1	−0.5	0
	BV2	0	0	1	0	0	1	0	0	1	0	0	1
IR4	BV1	0	−1	0	0	1	0	0	1	0	0	−1	0
IR5	BV1	0	−1	0	0	−1	0	0	−1	0	0	−1	0
IR6	BV1	1	0.5	0	1	0.5	0	−1	−0.5	0	−1	−0.5	0
	BV2	0	0	1	0	0	−1	0	0	−1	0	0	1
IR7	BV1	1	0.5	0	1	0.5	0	1	0.5	0	1	0.5	0
	BV2	0	0	1	0	0	−1	0	0	1	0	0	−1
IR8	BV1	0	−1	0	0	−1	0	0	1	0	0	1	0

$m_{ab}^{\mathrm{Ru}} = -0.19(1)\,\mu_B$, $m_c^{\mathrm{Ru}} = -0.43(2)\,\mu_B$, with their total moments 0.79(1) and 0.46(2), respectively. The thermal variation of the total magnetic moments of Er and Ru atoms along with their normalized magnetic moments behavior is shown in Fig. 12. It is evident that both Er and Ru moments show a slow increase from 40 K down to T_N whereas below T_N, both moments increase sharply. It is also to be noted that the Ru moment starts to saturate at low temperatures while the Er moment shows a continuous increase down to 1.6 K (lowest measured temperature) without any sign of saturation.

The derived magnetic structures corresponding to the IR7 and IR3 models of the BErRuO compound below and above T_N, respectively, are presented in Figs. 13(a) and 13(b). In both magnetic structures, in-plane magnetic interactions along the a and b directions are AFM and FM, respectively, while the out of plane interactions (along the c direction) are FM in IR3 and AFM in IR7. Moreover, within the Ru_2O_9 dimers, the coupling changes from FM (IR3) to AFM (IR7). It should be noted that in R = Nd [16], Ho [22], Tb (present), and Er (present) compounds, different magnetic moment orientations are observed. In the R = Nd and Ho (above T_{N2}) compounds, R and Ru magnetic moments are approximately orthogonal, whereas in the presently studied compounds, the moments are AFM coupled. This suggest that, although the RuO_6 octahedra have similar local geometry across these compounds, the effective R-Ru coupling is primarily governed by the rare earth dependent crystal-field parameters and anisotropic exchange interactions. The strong spin-orbit coupling of the $4f$ ions leads to markedly different anisotropies for different R ions, which can impose symmetry constraints on the allowed moment directions [28].

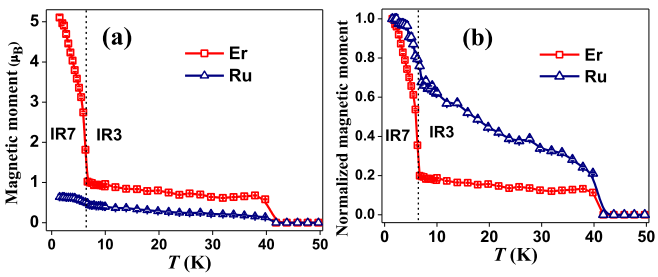

FIG. 12. Thermal variation of total (a) Er and Ru magnetic moments, and (b) normalized Er and Ru magnetic moments. The magnetic moments below and above T_N (represented by vertical dotted line) correspond to the IR7 and IR3 models, respectively.

IV. DISCUSSION

Within this family of BRRuO compounds, the magnetic structures have so far been reported in detail only for R = Nd and Ho. In BNdRuO, Nd orders ferromagnetically at 24 K. Below 18 K, not only FM Nd spins showed canting but FM Ru ordering within the Ru_2O_9 dimer was also observed [16]. This study shows the Nd orders first followed by the magnetic ordering of Ru. On the other hand, BHoRuO, a compound with heavy R = Ho, showed simultaneous and complex magnetic ordering of both Ho and Ru sublattices with strong $4f$-$4d$ coupling [22]. A similar strong $4f$-$4d$ coupling leads to the simultaneous ordering of the rare earth and Ru in both of the presently studied compounds, BTbRuO and BErRuO, each containing a heavy R atom. In these compounds, the possible exchange interactions comprise the superexchange pathways through R(Ru)-O2-Ru(R) and Ru-O1-Ru, and the direct exchange Ru-Ru. Looking at the determined magnetic structures [Fig. 7(a) and Fig. 13], it becomes clear that the AFM superexchange pathways linking

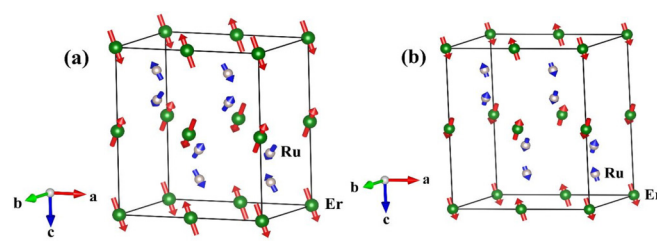

FIG. 13. IR7 and IR3 magnetic structures of BErRuO (a) below T_N and (b) above T_N, respectively. Ru moments are enlarged for better visibility.

R and Ru, $\angle R(\text{Ru})-\text{O2}-\text{Ru}(R) = 179.7^\circ$ and 179° (shown in Fig. 1), seem to be dominant over the other two competing exchange interactions, $\angle\text{Ru}-\text{O1}-\text{Ru} = 77.2^\circ$ and 76.2°, and $\text{Ru}-\text{Ru} = 2.519$ and 2.518 Å, for BTbRuO and BErRuO, respectively. This dominant interaction leads to the simultaneous AFM ordering of both R (Tb, Er) and Ru sublattices, demonstrating strong $4f$-$4d$ coupling. Moreover, the collinear (noncollinear) AFM Tb (Er) accompanied by the collinear (noncollinear) Ru magnetic ordering in BTbRuO (BErRuO) further suggests a strong coupling between $4f$ and $4d$ electrons. The presence of FM coupling within the Ru_2O_9 dimers, as found in BErRuO above T_N [Fig. 13(b)], however, points to the Ru-Ru exchange being of similar strength. This FM Ru ordering polarizes the Er moment and leads to the FM interaction among the Er spins along the c direction. Only when the super-superexchange interaction coupling between the rare earths along the c direction through Er-O2-Ru-O1-Ru-O2-Er becomes strong enough, is the magnetic ground state established in the BErRuO compound below T_N, which leads to a change of the magnetic coupling from FM (IR3) to AFM (IR7) along the c direction.

The derived magnetic moment values for both compounds and their variation with temperature are interesting. For BTbRuO, at 1.6 K, the derived Tb moment is $6.52(2)\,\mu_B$ which is close to the $Tb^{4+} = 7\,\mu_B$, indicating its +4 oxidation state in the compound, which is consistent with the literature [19]. In this context, Fig. 7(b) shows that the Tb moment seems to be saturated at low temperatures. Opposite to this, the determined Er magnetic moment of $5.1(1)\,\mu_B$ is much smaller than the theoretically expected $9\,\mu_B$ in BErRuO which can be attributed either to a crystal electric field effect or to the fact that the moment is not saturated at 1.6 K. The second possibility cannot be ruled out because the intensity of the magnetic reflections, which is proportional to the square of the magnetic moment, is still rising at 1.6 K (Fig. 10). A similar reduced Er moment is also reported in the literature in the related compounds [29,30]. Surprisingly, the $Ru^{4.5+}$ net moment $\sim 0.43(3)$ and $0.61(2)\,\mu_B$ at 1.6 K in both compounds is significantly reduced from its average spin-only magnetic moment value of $2.5\,\mu_B$. The reduced Ru moments are also reported in other related compounds like $Ba_3R^{3+}Ru_2^{+4.5}O_9$ (R = La, Y, and Nd) where magnetic moments of 1.4, 0.5, and $0.6\,\mu_B$, respectively, at 1.6 K are reported [16]. According to Ziat *et al.* [31], the Ru_2O_9 dimer in $Ba_3RRu_2O_9$ (R = Y, In, and Lu), isostructural to the presently studied compounds, behaves like a molecular unit due to significant orbital hybridization, resulting in a total spin $S = 1/2$ moment distributed over the two Ru sites. The Ru moments in the present case are in close agreement with a total spin of $S = 1/2$ per dimer indicating the role of orbital hybridization in the strong reduction of the Ru moment. The reduced Ru moment is not only limited to rare earth based $Ba_3RRu_2O_9$ compounds but also extended to other compounds like $Ba_3Co^{2+}Ru_2^{+5}O_9$ where much lower Ru $\sim 1.17\,\mu_B$ was reported than the expected spin-only value of $3\,\mu_B$. It was also explained by the hybridization effects with the O-2p states [32]. Substantial hybridization between the Ru-4d and O-2p states leads to a localization of the electrons not on the atomic but on the Wannier orbitals, with a large contribution coming from the nonmagnetic O-2p states.

In the literature, Basu *et al.* [22] reported magnetic ordering in BHoRuO at $T_{N1} \sim 50$ K with propagation vector $k_1 = (0.5, 0, 0)$, a temperature well above the magnetic ordering temperature ~ 10 K (T_{N2}) shown by dc susceptibility study. Below 10 K, the magnetic structure was characterized by the two propagation vectors, $k_1 = (0.5, 0, 0)$ and $k_2 = (0.25, 0.25, 0)$. Similar to BHoRuO, we have also observed magnetic ordering from NPD up to ~ 40 K in BErRuO; however, the magnetic structure is consistent with the $k = (0.5, 0, 0)$ throughout the magnetic ordering temperature range, as shown earlier. A very small Bragg peak intensity is noticed at $Q = 1.06$ Å^{-1} in the BTbRuO compound at 15 K ($> T_N$) which has disappeared at 50 K [Fig. 5(a)]. This also suggests that some magnetic ordering exists in this compound above T_N similar to BErRuO (present study) and BHoRuO [22]. The reflection at $Q = 1.06$ Å^{-1} is not a part of the $k = 0$ type magnetic structure of BTbRuO and it is not possible to refine any magnetic structure with a single magnetic reflection. However, its position can be indexed with the same propagation vector $k = (0.5, 0, 0)$ already found in the present BErRuO and reported BHoRuO [22]. It corresponds to the (0.5 0 2) reflection, which in the BErRuO [Fig. 9(b)] and BHoRuO [22] compounds represents the most intense magnetic reflection above T_N. On careful inspection, we could see a similar Bragg peak at the same scattering angle in the study of Doi *et al.* [20] on BTbRuO which was not indexed with $k = 0$. From this systematic comparison, it looks like all NPD-studied compounds of the BRRuO series with heavy rare earths exhibit magnetic ordering above T_N. Surprisingly, there are no signatures of magnetic order above T_N either from the present ac susceptibility measurements (Fig. 4) or from the reported specific heat studies [17,19]. It is worth mentioning that these two techniques are more sensitive than the dc susceptibility to catch the magnetic transitions [5,33]. We could understand that the magnetic ordering above T_N in these heavy rare earth members is very interesting as well as puzzling.

We have made one attempt to understand this puzzling magnetic ordering above T_N by preparing a BErRuO sample with 3% excess RuO_2 using the same preparation conditions as mentioned in the Experimental Details section. This excess RuO_2 was chosen considering its volatile nature. We call these two BErRuO compounds as BErRuO1 (without excess RuO_2) and BErRuO2 (with 3% excess RuO_2). The NPD patterns on BErRuO2 at all measured temperatures are shown in Fig. S5(a) in the SM [26]. It is interesting to note that there are no magnetic Bragg peaks at 10 K, at least within the certainty of the present NPD data which were measured with the same statistics as those of BErRuO1. For better understanding, we have shown the difference NPD data of 10 and 50 K for the BErRuO2 compound in Fig. 14 together with those of BErRuO1. It can be clearly seen that magnetic Bragg peaks, (0.5 0 2), (0.5 −1 3), (0.5 1 2), and (0.5 −2 −2) at $Q = 1.06$, 1.69, 1.85, and 2.39 Å^{-1}, respectively, persisting above $T_N \sim 6$ K in BErRuO1 have disappeared in BErRuO2. Rietveld refinements of the NPD data confirm the $P6_3/mmc$ crystal structure at all measured temperatures for this compound; the refinement of the 50 K NPD of BErRuO2 is shown in Fig. S5(b) in the SM [26]. The refinement infers a slightly higher ~ 1.4 wt % impurity phase of Er_2O_3 as compared to BErRuO1

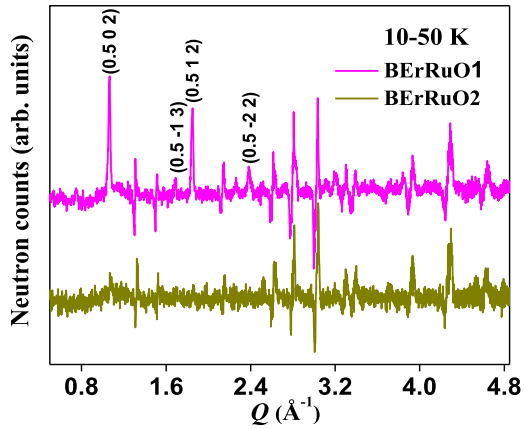

FIG. 14. The 10–50 K NPD data of BErRuO1 (pink) and BErRuO2 (olive) compounds. The patterns are vertically shifted for clarity.

having ∼0.6 wt % impurity phase. The derived lattice constants, $a = b = 5.869(2)$ Å and $c = 14.480(4)$ Å at 50 K, are found to be smaller than those determined for BErRuO1, $a = b = 5.874(2)$ Å and $c = 14.492(3)$ Å, at the same temperature. The smaller lattice constants are also evident from the XRD refinement results at 300 K (not shown). It may suggest that some Ru goes to the Er site, leaving extra unreacted Er_2O_3 behind. The ionic size of $Ru^{4.5+}$ (∼0.59 Å) is smaller than that of Er^{3+} (∼0.89 Å); therefore, as per the above assumption, the smaller lattice constants in BErRuO2 are expected. However, our attempt to check Er and Ru site disorder using Rietveld refinement of NPD data failed due to very similar neutron coherent scattering lengths, ∼7.79 and ∼7.03 fm, of the Er and Ru atoms, respectively. We also tried for site disorder using XRD, but no evidence was found, likely because the site disorder is below the detection limit of the XRD. Apart from these small differences, the Rietveld refinements of the 1.6 and 5 K NPD data of BErRuO2 are consistent with the magnetic structure of the BErRuO1 compound. Figure S5(c) in the SM [26] shows, for instance, the refined NPD data at 1.6 K. In addition, we could see extra Bragg peaks with small intensity at $Q = 0.84$ and 1.46 $Å^{-1}$ which are not present in the 5 K data. We could index these two Bragg peaks as (110) and (210) corresponding to the magnetic structure of Er_2O_3, consistent with the literature [34], which magnetically orders at 3.4 K. A similar but even smaller Bragg peak intensity can be found in BErRuO1 at $Q = 0.84$ $Å^{-1}$ corresponding to the same Er_2O_3 impurity phase [Fig. 10(a)]. However, due to the poor signal to noise ratio for this peak, we could not fit it. We can therefore attribute the anomaly at ∼3.6 K in the dc and ac susceptibility data [Figs. 3(a) and 4(b)] to the magnetic ordering of Er_2O_3. This anomaly is more pronounced in BErRuO2 as evident from the dc susceptibility data shown in Fig. S6 in the SM [26]. Thus, our analysis indicates that magnetic ordering above T_N can be suppressed by adding excess RuO_2 during sample preparation. It is worth mentioning that the IR7 magnetic structure below T_N is robust against this RuO_2 surplus.

V. SUMMARY AND CONCLUSIONS

By performing comprehensive temperature-dependent NPD experiments on $Ba_3RRu_2O_9$ (R = Tb, Er) compounds, we determined the unprecedented magnetic structure of $Ba_3ErRu_2O_9$ and also resolved contradictory issues related to the magnetic structure of $Ba_3TbRu_2O_9$. NPD results show that the magnetic structure of $Ba_3TbRu_2O_9$ is consistent with the propagation vector $k = 0$, where Tb and Ru spins are collinearly ordered in an AFM fashion along the c direction. This magnetic structure is in accordance with magnetic symmetry analysis and the magnetic space group formalism with $P6_3'/m'm'c$ being a maximal magnetic space group of the parent space group $P6_3/mmc$. Our results refute the magnetic structure and the large magnetic moment of Ru reported by Kushwaha *et al.* [21] for this compound. For BErRuO, a canted AFM ordering of both Er and Ru spins is observed, consistent with $k = (0.5, 0, 0)$. Different magnetic structures in both compounds suggest the role of magnetocrystalline anisotropy. Notably, in both compounds, R (Tb, Er) and Ru atoms order simultaneously demonstrating strong $4f$-$4d$ coupling. The observation of very weak magnetic ordering at temperatures above T_N adopting a different magnetic structure is similar to that found for BHoRuO [22]. One attempt to understand this intriguing feature by preparing the $Ba_3ErRu_2O_9$ compound with 3% excess RuO_2 revealed that the added excess RuO_2 suppresses the weak magnetic ordering above T_N; however, it preserves the magnetic structure below T_N. Despite this, single-crystal studies will be important to gain more insights into the interesting and puzzling features of these compounds.

ACKNOWLEDGMENTS

D.G. acknowledges the postdoctoral funding from the European Union's Horizon 2020 Research and Innovation Programme under the Marie Skłodowska-Curie Grant Agreement No. 101034266. D.G. is grateful to B. Veltel for his assistance in dc magnetization measurements performed at the Heinz Maier-Leibnitz Zentrum (MLZ).

DATA AVAILABILITY

The neutron powder diffraction data that support the findings of this work are openly available in Refs. [35,36], while all other data are available from the authors upon reasonable request.

[1] P. Yanda, N. Boudjada, J. Rodríguez-Carvajal, and A. Sundaresan, Exploring magnetism and magnetoelectric properties in the green phase of R_2BaCuO_5 (R = Er, Eu, Y, Tm, and Lu): The role of $4f$-$3d$ exchange coupling, Phys. Rev. B **109**, 104411 (2024).

[2] B. Rajeswaran, D. I. Khomskii, A. K. Zvezdin, C. N. R. Rao, and A. Sundaresan, Field-induced polar order at the Néel temperature of chromium in rare-earth orthochromites: Interplay of rare-earth and Cr magnetism, Phys. Rev. B **86**, 214409 (2012).

[3] T. Basu, A. Pautrat, V. Hardy, A. Loidl, and S. Krohns, Magnetodielectric coupling in a Ru-based 6H-perovskite, $Ba_3NdRu_2O_9$, Appl. Phys. Lett. **113**, 042902 (2018).

[4] T. Basu, V. Caignaert, S. Ghara, X. Ke, A. Pautrat, S. Krohns, A. Loidl, and B. Raveau, Enhancement of magnetodielectric coupling in 6H-perovskites $Ba_3RRu_2O_9$ for heavier rare-earth cations (R = Ho, Tb), Phys. Rev. Mater. **3**, 114401 (2019).

[5] D. Garg, A. Kumar, and S. M. Yusuf, Unraveling intricate magnetic behavior involving negative magnetization and exchange-bias in $ErFe_{0.5}Co_{0.5}O_3$, Phys. Rev. B **110**, 104401 (2024).

[6] D. Garg, A. Kumar, S. M. Yusuf, M. Skoulatos, S. N. Sarangi, D. Topwal, and Y. Su, Internal and external magnetic-field engineering of negative magnetization and exchange bias in $La_{1-x}Pr_xCrO_3(0.8 \leqslant x \leqslant 0.9)$, Phys. Rev. Mater. **9**, 054406 (2025).

[7] L. J. Chang, M. Prager, J. Perßon, J. Walter, E. Jansen, Y. Y. Chen, and J. S. Gardner, Magnetic order in the double pyrochlore $Tb_2Ru_2O_7$, J. Phys.: Condens. Matter **22**, 076003 (2010).

[8] C. R. Wiebe, J. S. Gardner, S. J. Kim, G. M. Luke, A. S. Wills, B. D. Gaulin, J. E. Greedan, I. Swainson, Y. Qiu, and C. Y. Jones, Magnetic Ordering in the Spin-Ice Candidate $Ho_2Ru_2O_7$, Phys. Rev. Lett. **93**, 076403 (2004).

[9] S. T. Ku, D. Kumar, M. R. Lees, W. T. Lee, R. Aldus, A. Studer, P. Imperia, S. Asai, T. Masuda, S. W. Chen, *et al.*, Low temperature magnetic properties of $Nd_2Ru_2O_7$, J. Phys.: Condens. Matter **30**, 155601 (2018).

[10] Y. Doi, Y. Hinatsu, A. Nakamura, Y. Ishii, and Y. Morii, Magnetic and neutron diffraction studies on double perovskites A_2LnRuO_6 (A = Sr, Ba; Ln = Tm, Yb), J. Mater. Chem. **13**, 1758 (2003).

[11] D. T. Adroja, S. Sharma, C. Ritter, A. D. Hillier, D. Le, C. V. Tomy, R. Singh, R. I. Smith, M. Koza, A. Sundaresan, *et al.*, Muon spin rotation and neutron scattering investigations of the B-site ordered double perovskite Sr_2DyRuO_6, Phys. Rev. B **101**, 094413 (2020).

[12] H. Guo, C. Ritter, and A. C. Komarek, Direct determination of the spin structure of $Nd2Ir_2O_7$ by means of neutron diffraction, Phys. Rev. B **94**, 161102(R) (2016).

[13] H. Guo, C. Ritter, and A. C. Komarek, Magnetic structure of $Tb_2Ir_2O_7$ determined by powder neutron diffraction, Phys. Rev. B **96**, 144415 (2017).

[14] E. Lefrançois, V. Simonet, R. Ballou, E. Lhotel, A. Hadj-Azzem, S. Kodjikian, P. Lejay, P. Manuel, D. Khalyavin, and L. C. Chapon, Anisotropy-tuned magnetic order in pyrochlore iridates, Phys. Rev. Lett. **114**, 247202 (2015).

[15] M. Hase, A. Dönni, and V. Y. Pomjakushin, Magnetic structures of nearly isostructural Tb_3RuO_7 and Nd_3RuO_7: Appearance of a partially disordered state only in the Tb compound, Phys. Rev. B **104**, 214430 (2021).

[16] M. S. Senn, S. A. J. Kimber, A. M. Arevalo Lopez, A. H. Hill, and J. P. Attfield, Spin orders and lattice distortions of geometrically frustrated 6H-perovskites $Ba_3B'Ru_2O_9$ (B' = La^{3+}, Nd^{3+}, and Y^{3+}), Phys. Rev. B **87**, 134402 (2013).

[17] Y. Doi and Y. Hinatsu, Magnetic and calorimetric studies on $Ba_3LnRu_2O_9$ (Ln = Gd, Ho–Yb) with 6H-perovskite structure, J. Mater. Chem. **12**, 1792 (2002).

[18] Y. Doi, Y. Hinatsu, Y. Shimojo, and Y. Ishii, Crystal structure and magnetic properties of 6H-perovskite $Ba_3NdRu_2O_9$, J. Solid State Chem. **161**, 113 (2001).

[19] Y. Doi, M. Wakeshima, Y. Hinatsu, A. Tobo, K. Ohoyama, and Y. Yamaguchi, Magnetic and calorimetric studies on 6H-perovskite $Ba_3TbRu_2O_9$, J. Alloys Compd. **344**, 166 (2002).

[20] Y. Doi, M. Wakeshima, Y. Hinatsu, A. Tobo, K. Ohoyama, and Y. Yamaguchi, Crystal structures and magnetic properties of the 6H-perovskites $Ba_3LnRu_2O_9$ (Ln = Ce, Pr and Tb), J. Mater. Chem. **11**, 3135 (2001).

[21] E. Kushwaha, G. Roy, A. M. dos Santos, M. Kumar, S. Ghosh, T. Heitmann, and T. Basu, Unconventional S-orbital state of Tb and cooperative Ru($4d$)-Tb($4f$) spin-ordering in the strongly correlated $4d$–$4f$ system $Ba_3TbRu_2O_9$, J. Mater. Chem. C **13**, 15384 (2025).

[22] T. Basu, V. Caignaert, F. Damay, T. W. Heitmann, B. Raveau, and X. Ke, Cooperative Ru($4d$) –Ho($4f$) magnetic ordering and phase coexistence in the 6H perovskite multiferroic $Ba_3HoRu_2O_9$, Phys. Rev. B **102**, 020409(R) (2020).

[23] H. Rietveld, A profile refinement method for nuclear and magnetic structures, J. Appl. Crystallogr. **2**, 65 (1969).

[24] J. Rodríguez-Carvajal, Recent advances in magnetic structure determination by neutron powder diffraction, Physica B **192**, 55 (1993).

[25] M. I. Aroyo, J. M. Perez-Mato, C. Capillas, E. Kroumova, S. Ivantchev, G. Madariaga, A. Kirov, and H. Wondratschek, Bilbao Crystallographic Server: I. Databases and crystallographic computing programs, Z. Kristallogr. - Cryst. Mater. **221**, 15 (2006).

[26] See Supplemental Material at http://link.aps.org/supplemental/10.1103/pbtn-g5wz for the details of Rietveld refinement of the XRD data at 300 K for both compounds, structural parameter details from XRD at 300 K and NPD at 1.6 K for both compounds, dc susceptibility data of both compounds over the temperature range of 1.8–380 K, NPD data of BTbRuO compound at 15 and 50 K in the paramagnetic state, additional Rietveld refined NPD results on BTbRuO, NPD data of the BErRuO2 compound (with 3% excess RuO_2) and the Rietveld refinement of 50 and 1.6 K NPD data, and dc susceptibility data of BErRuO2.

[27] A. S. Wills, A new protocol for the determination of magnetic structures using simulated annealing and representational analysis (SARAh), Physica B **276–278**, 680 (2000).

[28] V. Hardy, V. Caignaert, F. Veillon, F. Guillou, Y. Bréard, B. Raveau, M. Avdeev, and B. Gonano, Relationship between crystalline anisotropy and magnetic structure in the series Ba_2LnFeO_5 (Ln = Tb, Dy, Ho, Er, Yb), Phys. Rev. B **112**, 144425 (2025).

[29] N. Taira, M. Wakeshima, Y. Hinatsu, A. Tobo, and K. Ohoyama, Magnetic structure of pyrochlore-type $Er_2Ru_2O_7$, J. Solid State Chem. **176**, 165 (2003).

[30] Y. Zhou, M.-K. Lee, S. Hammouda, S. Devi, S.-I. Yano, R. Sibille, O. Zaharko, W. Schmidt, K. Schmalzl, K. Beauvois, *et al.*, Ground-state magnetic structures of topological kagome metals RV_6Sn_6 (R = Tb, Dy, Ho, Er), Phys. Rev. Res. **6**, 043291 (2024).

[31] D. Ziat, A. A. Aczel, R. Sinclair, Q. Chen, H. D. Zhou, T. J. Williams, M. B. Stone, A. Verrier, and J. A. Quilliam, Frustrated spin-1/2 molecular magnetism in the mixed-valence antiferromagnets $Ba_3MRu_2O_9$ (M = In, Y, Lu), Phys. Rev. B **95**, 184424 (2017).

[32] S. V. Streltsov, Magnetic moment suppression in $Ba_3CoRu_2O_9$: Hybridization effect, Phys. Rev. B **88**, 024429 (2013).

[33] N. Taira, M. Wakeshima, and Y. Hinatsu, Magnetic susceptibility and specific heat studies on heavy rare earth ruthenate pyrochlores $R_2Ru_2O_7$ (R = Gd-Yb), J. Mater. Chem. **12**, 1475 (2002).

[34] R. M. Moon, W. C. Koehler, H. R. Child, and L. J. Raubenheimer, Magnetic structures of Er_2O_3 and Yb_2O_3, Phys. Rev. **176**, 722 (1968).

[35] D. Garg, C. Ritter, and Y. Su, Investigations of Ru ordering and magnetic structure of 6H-perovskite, $Ba_3TbRu_2O_9$, Institut Laue-Langevin (ILL) (2024), doi:10.5291/ILL-DATA.5-31-3048.

[36] D. Garg, C. Ritter, and Y. Su, Study of magnetic structure of triangular lattice $Ba_3ErRu_2O_9$ using neutron diffraction, Institut Laue-Langevin (ILL) (2025), doi:10.5291/ILL-DATA.5-31-3081.